

Magnetization switching by current in an elemental ferromagnetic single layer

Yanyan Yang & Weiwei Lin*

Key Laboratory of Quantum Materials and Devices of Ministry of Education, School of Physics, Southeast
University, Nanjing 211189, China.

*e-mail: wlin@seu.edu.cn

(Submitted 23 February 2025; revised 29 July 2025)

Current-induced magnetization switching, a fundamental phenomenon related to spin-transport of electrons, enables non-voltaic and fast information write, facilitating applications in low-power memory and logic devices. However, magnetization switching by spin-orbit torques is usually attributed to current flowing in the nonmagnetic metal layer of multilayers or in magnetic alloys with heavy elements. Here, we report perpendicular magnetization switching induced by current flowing in an elemental ferromagnet nickel single layer. This prototype structure demonstrates that current-induced magnetization switching is a general phenomenon of magnet. The results suggest that the current induces an effective transverse magnetic field with an out-of-plane component leading to the magnetization switching, different to the conventional spin-orbit torques. Our work opens the new insight and reveals the intrinsic mechanism of current-induced torques.

In the 1970s, Berger et al. predicted in-plane current driven perpendicular magnetization reversal via magnetic domain wall motion¹⁻³. Experimentally, in-plane current-induced deterministic switching of perpendicular magnetization has been reported in magnetic/nonmagnetic metal (NM) multilayers such as Pt/Co/Pt^{4,5}, and later, reversible current-induced magnetization switching (CIMS) has been observed in Pt/Co/ AlO_x ^{6,7} and Ta/CoFeB/MgO⁸ in which the switching polarity depends on the direction of the applied magnetic field along the current. The perpendicular magnetization switching is ascribed to spin-orbit torques (SOTs) from the spin Hall effect (SHE) in the adjacent NM layer with large spin-orbit coupling (SOC)^{7,8} and/or the Rashba effect at the interfaces⁶. Various topological insulators (e.g. BiSbTe^{9,10}, Bi₂Se₃¹¹), antiferromagnets (e.g. PtMn¹²) and van der Waals materials (e.g. WTe₂^{13,14}) with large SOC have been utilized in SOT switching. However, the multilayers with a 4d transition metal Zr layer which are of weak SOC and small spin Hall angle have also been investigated similar CIMS, attributed to orbital Hall effect (OHE) in Zr^{15,16}.

CIMS has been also observed in single magnetic layers without the adjacent NM metal layer with SHE, such as non-centrosymmetric ferromagnetic semiconductor (Ga,Mn)As^{17,18}, ferromagnetic metals *L*10-FePt^{19,20} and CoPt²¹ alloys, rare earth ferrimagnetic CoTb^{22,23} and FeTb²⁴ alloys, and non-collinear antiferromagnetic semimetal Mn₃Sn²⁵. However, heavy elements with large SOC are included in most alloys. Low crystal symmetry¹⁷⁻²¹, composition gradient^{21,23,24} or locally asymmetric magnetic sublattices¹³ have been suggested to be crucial for the switching behavior. CIMS in the thick single magnetic layer is mainly attributed to bulk spin torques due to large SOC^{19,20} but the exact mechanisms remain unclear so far. Can perpendicular magnetization be switched by current in a single magnetic layer without large SOC ?

Here, we report the perpendicular magnetization switching induced by current flowing in a single elemental ferromagnetic nickel layer. This is the simplest and basic structure to realize CIMS without large SOC of heavy elements and absence of crystal asymmetry, composition gradient and magnetic sublattices. The result is crucial to verify the intrinsic mechanism of CIMS. We deposited the Ni films on undoped Si(100) substrates using magnetron sputtering at

room temperature and patterned Hall bars (shown in Fig. S1) via photo-lithography and ion etching.

As shown in Fig. 1a, the current \mathbf{I} is injected in the Ni layer along x axis and a magnetic field \mathbf{H}_x is applied parallel to the current. The perpendicular magnetization \mathbf{M} of Ni can be switched by the injected current. Figure 1b shows the anomalous Hall resistance R_{xy} loops with out-of-plane magnetic field H_z of the device of 5.4 nm thick Ni layer and about 1 nm thick naturally oxidized NiO_x on surface. The negative R_{xy} refers to the Ni magnetization pointing to up, due to negative anomalous Hall angle of Ni. The R_{xy} loops become square as the temperature T decreases below 200 K, see also Fig. S2a. Both the remanence of the anomalous Hall resistance at zero out-of-plane field R_{xy}^0/R_{xy}^s and the coercivity H_c increase significantly with the T decreasing below 200 K, as shown in Fig. S2b. This indicates the transition of the magnetic easy axis of the Ni layer from in-plane to out-of-plane around 200 K due to magnetoelastic anisotropy^{26,27}. The magnetization remanence is 100% and the coercivity is 45 mT at 5 K. Figure 1c shows the current-induced switching in the Ni(5.4)/NiO_x(1) device at 50 K with the applied field H_x along x axis. More current-induced switching loops for various H_x at 50 K and 150 K are shown in Fig. S3. The anomalous Hall switching loop is counter-clockwise for the positive H_x , but is clockwise for the negative H_x . It indicates that the Ni magnetization favorites pointing to up (down) as the current is anti-parallel (parallel) to the field, as shown in Fig. 1a. The polarity of magnetization switching is the same as that of Pt/Co/AlO_x⁶ but opposite to that of Ta/CoFeB/MgO⁸. The switching polarity may be related to current-induced domain wall motion^{28,29} in Ni with a positive Dzyaloshinskii-Moriya interaction (DMI)³⁰. No magnetization switching induced by current is observed as the applied field is along y axis.

Temperature dependence of current-induced switching

Figure 2a represents the current-induced switching loops of the Ni(5.4)/NiO_x(1) device under $\mu_0 H_x = 10$ mT at several temperatures. The critical current I_c and current density J_c decreases by a factor of 10 with the T increasing from 6 K to 200 K, as shown in Fig. 2b. J_c is about 2×10^7 A cm⁻² at 200 K. This behavior is similar to that in single layers of magnetic alloys¹⁸ and magnetic/NM multilayers^{13,14}, related to the reduce of the energy barriers and the

propagation field of thermal excited magnetic domain wall motion as the T increases⁵. Figure 2c shows the H_x dependence of I_c (J_c) at 6 K. The J_c decreases as the magnitude of H_x increases, similar to the behaviors in the magnetic/NM multilayers^{6,9,12} and the magnetic alloys²⁰. The in-plane magnetic field turns the in-plane orientation of the magnetic moments within the domain walls and induces asymmetric propagation of the domain walls²⁸⁻³¹. One may see from Fig. 2c that the magnetization prefers pointing to up (down) as the current is anti-parallel (parallel) to the field. Figure 2d shows the H_x dependence of current-induced switching ratio of magnetization $\Delta R_{xy}/2 R_{xy}^S$ at several temperatures. The switching ratio of magnetization increases and then decreases with increasing H_x , having a maximum at the field magnitude of about 10 mT at 6 K. This behavior is similar to the previous results in magnetic multilayers and alloys^{12,20}. The increase of the switching ratio is due to the small in-plane field promotes the propagation of domain walls. Large in-plane field leads to the tilt of magnetization and reduces the perpendicular magnetization component for switching, resulting in the decrease of switching ratio. We have observed full magnetization switching induced by current in Ni at 6 K, as shown in Fig. S4. The maximum of current-induced switching ratio of magnetization increases with decreasing the T ³². It is also resulted from the increase of the perpendicular magnetization remanence with decreasing the T (see Fig. S2b) due to the enhancement of perpendicular magnetic anisotropy (PMA) at low temperatures.

Thickness dependence of current-induced switching

The NiO_x on the surface is not antiferromagnetic, because no exchange bias is observed for the Ni/NiO_x devices after in-plane field cooling down to 6 K, as shown in Fig. S5. In addition to Ni/NiO_x we also measured the CIMS in devices of Ni layer with about 3 nm thick naturally oxidized AlO_x layer. Figure 3a shows anomalous Hall resistance loops with out-of-plane fields in Ni(t_{Ni})/AlO_x(3) for several Ni thickness t_{Ni} at 6 K. The Ni shows PMA for the Ni layer thickness from 5 to 8 nm. Figure 3b shows current-induced switching loop for several Ni layer thicknesses at 6 K under $\mu_0 H_x = 10$ mT. It indicates the current switching ratio of magnetization is largest for the 6 nm thick Ni layer. Figure 3c shows the Ni layer thickness dependence of critical current density under $\mu_0 H_x = 10$ mT at 6 K. The J_c increases by 4 times with the Ni thickness from 5 nm to 8 nm, suggesting that the efficiency of current-induced torques is larger for the thinner Ni layer. This is similar to the interface dominated spin torques³³, but contrast to the bulk spin torques where J_c almost does not change²² or decreases¹³ with the magnetic layer thickness increasing. This indicates that the interfaces of Si/Ni and Ni/AlO_x

play a crucial role in CIMS of Ni. As the Ni thickness decreases, the influence of the Si/Ni and Ni/AIO_x interfaces dominates, leading to an enhancement in the efficiency of CIMS. The contributions of the Si/Ni and Ni/AIO_x interfaces could be asymmetric. From the Ni thickness dependence of J_c , we suggest that CIMS does not mainly from the self-induced bulk spin torques in Ni layer. The CIMS in the Ni layer originates mainly from current-induced torques at the Ni/insulator interfaces.

Current-induced effective magnetic field

To further explore the mechanism of CIMS in the Ni, we quantitatively evaluate the current-induced effective magnetic field^{5,29}. We measured the R_{xy} vs H loops in the Ni with various I and H_x . Figure 4a shows the R_{xy} loops with sweeping field H at $\theta = 85^\circ$ (θ is the angle of the applied field H relative to the normal of the surface in yz plane, see Fig. S6a) in the Ni/NiO_x at 14 K with $\mu_0 H_x = -8$ mT. The R_{xy} loops corresponding to positive (negative) currents shift to the left (right) under $\mu_0 H_x = -8$ mT. There is no loop shift without the applied field along x axis, as shown in Fig. S6b. For the same current, the loop shift with $\mu_0 H_x = 8$ mT is opposite to that with $\mu_0 H_x = -8$ mT, as shown in Fig. S6c. As the current magnitude increases, the R_{xy} loops become narrow. One may notice from Fig. 4a that with $\mu_0 H_x = -8$ mT large positive (negative) current induces dip (peak) at low field of loop which does not appear for the small current. However, as shown in Fig. S6c, with $\mu_0 H_x = 8$ mT large positive (negative) current induces peak (dip) at low field of loop. It suggests the roles of both the current and the applied field H_x on the magnetization reversal process. The current dependence of the switching field is shown in Fig. 4b, where H_L and H_R refer to the switching field for field descending branch and ascending branch, respectively. The switching (coercive) field decreases remarkably with increasing the current, indicating current-induced torques and Joule heating helps the magnetization switching and thermal excited magnetic domain wall motion^{4,5}. The R_{xy} loop shift along the H axis reverses with current, indicating the existence of current-induced effective magnetic field H^{eff} which depends on the current direction. The current-induced effective magnetic field $H^{\text{eff}} = -H^{\text{shift}} = -\frac{1}{2}(H_L + H_R)$, where H^{shift} is the shift field of R_{xy} vs H loops. As shown in Fig. 4c, the magnitude of H^{eff} increases with the current and saturated above 15 mA. The sign (direction) of H^{eff} reverses with either the current direction or the applied field direction along x axis. This is very different to the Oersted field and the Rashba field. The H^{eff} is close to $+y$ ($-y$) direction as the current is anti-parallel (parallel) to the applied field along x axis. The current-induced effective field can be expressed as $\mu_0 H^{\text{eff}} = \chi J_c$, where χ is the

coefficient of current-induced effective field. For the applied field of 8 mT along x axis, the coefficient of current-induced effective field χ in Ni is about $1.1 \times 10^{-7} \text{ mT A}^{-1} \text{ cm}^2$ at 14 K.

To verify the direction of current-induced effective field, we measured the R_{xy} vs H loops in the Ni/NiO_x at 14 K for several angles θ with various I . As shown in Figs. S6d-6f, the current-induced loop shift can also be observed at $\theta = 60^\circ$, 30° , and 0° . One may see from Fig. S6g that the sign of shift field H^{shift} reverses with the current direction and the magnitude of H^{shift} increases with θ . The $H^{\text{shift}}(\theta)$ follows the $H^{\text{shift}}(0)/\cos\theta$ behavior, where $H^{\text{shift}}(0)$ is the shift field at $\theta = 0^\circ$, as shown in Fig. S6h. It indicates that the current-induced effective field is close to +y (-y) direction with a +z (-z) component as the current is anti-parallel (parallel) to the applied field along x axis. The current-induced effective field leads to the torques for the perpendicular magnetization switching.

To confirm the out-of-plane component of the current-induced effective field, we measured the R_{xy} vs H_z loops in the Ni/NiO_x at 6 K with various I and H_x . As shown in Fig. S7a, the current induces a clear shift of R_{xy} loops in the Ni/NiO_x with $\mu_0 H_x = 8 \text{ mT}$. It can be seen clearly that the R_{xy} loops corresponding to positive (negative) currents shift to the right (left) under $\mu_0 H_x = 8 \text{ mT}$, and the shift direction reverses with $\mu_0 H_x = -8 \text{ mT}$, as shown in Fig. S7b. As the current increases, the loops become narrow and the perpendicular remanence magnetization decreases, indicating that the current reduces the energy barriers and the propagation field of thermal excited magnetic domain wall motion including the contributions of Joule heating^{4,5,29}. The anomalous Hall loop shift along the H_z axis reverses with current, indicating the out-of-plane component of current-induced effective field H_z^{eff} which depends on the current direction. This is similar to the results in CoPt alloy³⁴. The current dependence of the switching field H_L and H_R is shown in Figs. S7e and 7f for 8 mT and -8 mT, respectively. The switching (coercive) field decreases remarkably with increasing the current, indicating current-induced torques and Joule heating helps the magnetization switching and thermal excited magnetic domain wall motion^{4,5}. The out-of-plane component of current-induced effective field $H_z^{\text{eff}} = -H_z^{\text{shift}} = -\frac{1}{2}(H_L + H_R)$, where H_z^{shift} is the shift field of R_{xy} vs H_z loops. The magnitude of H_z^{eff} is proportional to the current (in the measured current range) and the sign of H_z^{eff} reverses with either the current direction or the applied field direction along x axis, as shown in Fig. S7g. The H_z^{eff} points to up (down) as the current is anti-parallel (parallel) to the applied field along x axis. As shown in Figs. S7c and 7d, the current dependence of R_{xy}^0 at zero H_z show a loop behavior and reverses for the opposite H_x , indicating that the current-induced effective field results in the perpendicular magnetization switching.

The applied magnetic field along x direction induces a tilt of out-of-plane magnetization and magnetization component along x direction within the chiral domain walls, as sketched in Fig. S8. Due to the inversion symmetry breaking by the substrate and surface, the effective field close to y direction with a z component can be induced by current around the chiral domain walls at the Ni/insulator interfaces with interfacial Dzyaloshinskii-Moriya interaction^{28,29}. The current-induced effective magnetic field breaks the symmetry of up and down magnetization. The reversed magnetic domains expand due to the current-induced effective field, resulting in the perpendicular magnetization switching.

Conclusion and outlook

We have demonstrated the current induced perpendicular magnetization switching in an elemental ferromagnetic single layer, which is the basic structure to uncover the hidden mechanism of current-induced torques. The results prove that even for Ni single layer without large bulk SOC can achieve CIMS. This indicates CIMS does not require the NM layers with SHE and OHE, and the heavy elements in magnetic alloys with large SOC. Our work reveals that CIMS can be achieved without requiring SHE or OHE, nor the presence of heavy elements in magnetic alloys. This is not limited to specific materials and structures but represents a universal phenomenon in magnets. The results suggest that the current-induced effective transverse magnetic field at the Ni/insulator interfaces plays a dominant role in CIMS. This mechanism is intrinsic and general, applicable for the previous studied systems of magnetic multilayers and alloys. Our work suggests the CIMS can be realized without of complex fabrication processes for alloys and oxides, which is accessible for the integration. Enhancement of PMA at room temperature, the switching ratio free of field and reducing the critical current density for switching are essential to the applications of magnetic memory and logic devices based on current-induced torques.

References

- 1 Berger, L. Prediction of a domain-drag effect in uniaxial, non-compensated, ferromagnetic metals. *J. Phys. Chem. Solids* **35**, 947-956 (1974).
- 2 Carr, W. J., Jr. Propagation of magnetic domain walls by a self-induced current distribution. *J. Appl. Phys.* **45**, 394-396 (1974).
- 3 Charap, S. H. Interaction of a magnetic domain wall with an electric current. *J. Appl. Phys.* **45**, 397-402 (1974).
- 4 Lin, W. W. *et al.* Magnetization switching induced by in-plane current with low density in Pt/Co/Pt sandwich. *J. Appl. Phys.* **99**, 08G518 (2006).
- 5 Xie, K. X., Lin, W. W., Sun, H. C., Nie, Y. & Sang, H. Time dependence of magnetization reversal influenced by current in perpendicularly magnetized Co/Pt thin film. *J. Appl. Phys.* **104**, 083907 (2008).
- 6 Miron, I. M. *et al.* Perpendicular switching of a single ferromagnetic layer induced by in-plane current injection. *Nature* **476**, 189-193 (2011).
- 7 Liu, L., Lee, O. J., Gudmundsen, T. J., Ralph, D. C. & Buhrman, R. A. Current-induced switching of perpendicularly magnetized magnetic layers using spin torque from the spin Hall effect. *Phys. Rev. Lett.* **109**, 096602 (2012).
- 8 Liu, L. *et al.* Spin-torque switching with the giant spin Hall effect of tantalum. *Science* **336**, 555-558 (2012).
- 9 Fan, Y. *et al.* Magnetization switching through giant spin-orbit torque in a magnetically doped topological insulator heterostructure. *Nat. Mater.* **13**, 699-704 (2014).
- 10 Yasuda, K. *et al.* Current-nonlinear Hall effect and spin-orbit torque magnetization switching in a magnetic topological insulator. *Phys. Rev. Lett.* **119**, 137204 (2017).
- 11 Han, J. *et al.* Room-temperature spin-orbit torque switching induced by a topological insulator. *Phys. Rev. Lett.* **119**, 077702 (2017).
- 12 Fukami, S., Zhang, C., DuttaGupta, S., Kurenkov, A. & Ohno, H. Magnetization switching by spin-orbit torque in an antiferromagnet-ferromagnet bilayer system. *Nat. Mater.* **15**, 535-541, (2016).
- 13 Shin, I. *et al.* Spin-orbit torque switching in an all-van der waals heterostructure. *Adv. Mater.* **34**, 2101730 (2022).
- 14 Kao, I. H. *et al.* Deterministic switching of a perpendicularly polarized magnet using unconventional spin-orbit torques in WTe₂. *Nat. Mater.* **21**, 1029-1034 (2022).
- 15 Zheng, Z. C. *et al.* Magnetization switching driven by current-induced torque from weakly spin-orbit coupled Zr. *Phys. Rev. Res.* **2**, 013127 (2020).
- 16 Yang, Y. *et al.* Orbital torque switching in perpendicularly magnetized materials. *Nat. Commun.* **15**, 8645 (2024).
- 17 Yamanouchi, M., Chiba, D., Matsukura, F. & Ohno, H. Current-induced domain-wall switching in a ferromagnetic semiconductor structure. *Nature* **428**, 539-542 (2004).
- 18 Jiang, M. *et al.* Efficient full spin-orbit torque switching in a single layer of a perpendicularly magnetized single-crystalline ferromagnet. *Nat. Commun.* **10**, 2590 (2019).
- 19 Tang, M. *et al.* Bulk Spin torque-driven perpendicular magnetization switching in L10 FePt single layer. *Adv. Mater.* **32**, 2002607 (2020).
- 20 Liu, L. *et al.* Electrical switching of perpendicular magnetization in a single ferromagnetic layer. *Phys. Rev. B* **101**, 220402 (2020).
- 21 Liu, L. *et al.* Current-induced self-switching of perpendicular magnetization in CoPt single layer. *Nat. Commun.* **13**, 3539 (2022).

- 22 Zhang, R. Q. *et al.* Current-induced magnetization switching in a CoTb amorphous single layer. *Phys. Rev. B* **101**, 214418 (2020).
- 23 Zheng, Z. *et al.* Field-free spin-orbit torque-induced switching of perpendicular magnetization in a ferrimagnetic layer with a vertical composition gradient. *Nat. Commun.* **12**, 4555 (2021).
- 24 Liu, Q., Zhu, L., Zhang, X. S., Muller, D. A. & Ralph, D. C. Giant bulk spin-orbit torque and efficient electrical switching in single ferrimagnetic FeTb layers with strong perpendicular magnetic anisotropy. *Appl. Phys. Rev.* **9**, 021402 (2022).
- 25 Hu, S. *et al.* Efficient perpendicular magnetization switching by a magnetic spin Hall effect in a noncollinear antiferromagnet. *Nat. Commun.* **13**, 4447 (2022).
- 26 Gerber, A. *et al.* Effect of surface scattering on the extraordinary Hall coefficient in ferromagnetic films. *Phys. Rev. B* **65**, 054426 (2002).
- 27 Riss, O., Tsukernik, A., Karpovsky, M. & Gerber, A. Reorientation phase transition and sensitivity of the extraordinary Hall-effect-based sensors. *J. Magn. Magn. Mater.* **298**, 73-77 (2006).
- 28 Thiaville, A., Rohart, S., Jué, É., Cros, V. & Fert, A. Dynamics of Dzyaloshinskii domain walls in ultrathin magnetic films. *Europhys. Lett.* **100**, 57002 (2012).
- 29 Lee, O. J. *et al.* Central role of domain wall depinning for perpendicular magnetization switching driven by spin torque from the spin Hall effect. *Phys. Rev. B* **89**, 024418 (2014).
- 30 Allenspach, R. *et al.* Dzyaloshinskii-Moriya interaction in Ni/Cu(001). *Phys. Rev. B* **110**, 014402 (2024).
- 31 Je, S.-G. *et al.* Asymmetric magnetic domain-wall motion by the Dzyaloshinskii-Moriya interaction. *Phys. Rev. B* **88**, 214401 (2013).
- 32 Jiang, M. *et al.* Efficient full spin-orbit torque switching in a single layer of a perpendicularly magnetized single-crystalline ferromagnet. *Nat. Commun.* **10**, 2590 (2019).
- 33 Lee, K.-S., Lee, S.-W., Min, B.-C. & Lee, K.-J. Threshold current for switching of a perpendicular magnetic layer induced by spin Hall effect. *Appl. Phys. Lett.* **102**, 112410 (2013).
- 34 Xie, X. *et al.* Controllable field-free switching of perpendicular magnetization through bulk spin-orbit torque in symmetry-broken ferromagnetic films. *Nat. Commun.* **12**, 2473 (2021).

Methods

Sample fabrication and characterization

The undoped Si(100) substrates were cleaned with hydrofluoric acid before the film deposition to remove the oxidizes on surface. The Ni films were deposited on the insulating Si substrates at room temperature using a dc magnetron sputtering with a base pressure of 7.8×10^{-6} Pa and an Ar pressure of 0.3 Pa. By measuring the resistance of the film, we estimate that approximately 1 nm NiO_x layer is on top by natural oxidation in air. For the Ni/AlO_x devices, a 2 nm thick Al layer was sputtered on the Ni layer, followed by natural oxidation to form approximately 3 nm AlO_x on top. The small angle X-ray reflectivity as shown in Fig. S1b indicates the small roughness of the Ni films. X-ray diffraction (XRD) shows the Ni film is (111) textured. The Ni films were patterned by UV photo-lithography and Ar ion milling into Hall bar devices with a stripe size of $20 \times 5 \mu\text{m}^2$, see Fig. S1a.

Electrical transport measurements

For the CIMS measurement, a pulsed electrical current with a duration of 1 ms was applied using a current source Keithley 6221. a d.c. current I_{dc} of 0.1 mA was applied 1s after the current pulse and the Hall voltage V_{dc} was recorded using a nanovoltmeter Keithley 2182A. The Hall resistance $R_{\text{xy}} = V_{\text{dc}}/I_{\text{dc}}$ was determined to characterize the magnetization state.

Current-induced anomalous Hall loop shift was measured to characterize the current-induced effective field. The anomalous Hall effect of the Ni devices was measured by sweeping the magnetic field and applying a constant field parallel to the current. A pulsed current with 1 ms duration was applied by Keithley 6221 and subsequently a dc current of 0.1 mA was applied 1s after the pulsed current to measure the Hall voltage.

Acknowledgements

We acknowledge support from the National Key Research and Development Program of China 2023YFA1406600.

Author contributions

W.L. conceived and supervised the work and developed physics model. Y.Y. fabricated the samples and performed the measurements. Both authors analyzed the data, discussed the results and wrote the manuscript.

Competing interests The authors declare no competing interests.

Additional information

Correspondence and requests for materials should be addressed to Weiwei Lin.

Figures and legends

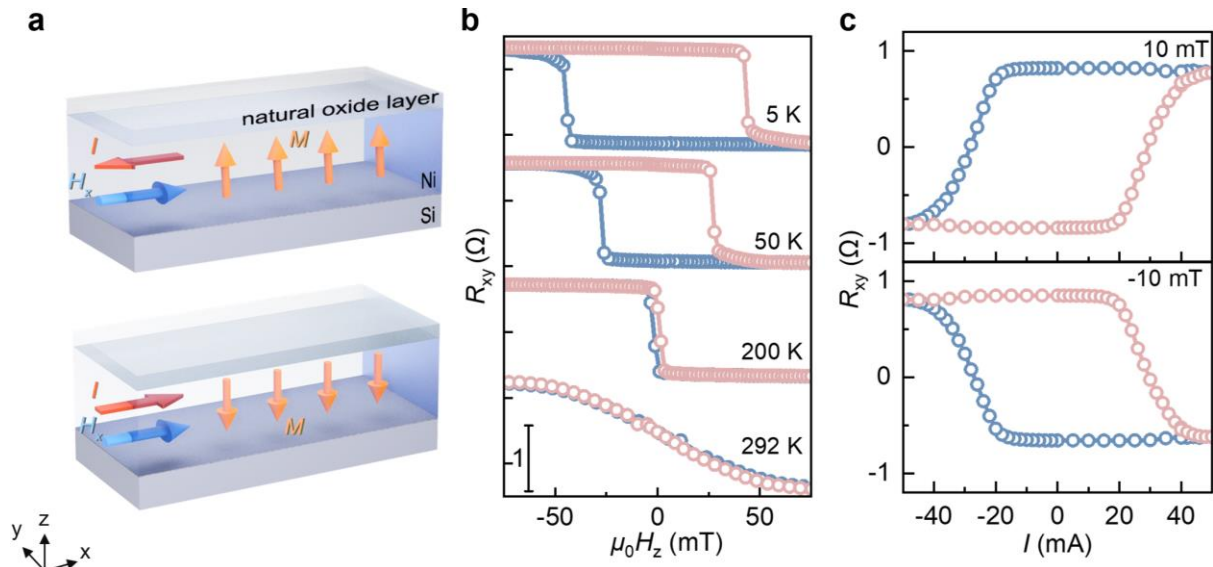


Fig. 1 | Current-induced magnetization switching in Ni layer. **a**, Schematic of current-induced magnetization switching in the Si/Ni/natural oxide layer structure. The magnetization is switched from up to down as the current is reversed from -x direction to +x direction, with a magnetic field applied along the +x direction. **b**, Anomalous Hall resistance loops with out-of-plane magnetic field at several temperatures for a Si/Ni(5.4)/NiO_x(1) device. **c**, Anomalous Hall resistance loops for the Si/Ni(5.4)/NiO_x(1) at 50 K by sweeping the pulsed currents under the applied magnetic field $\mu_0 H_x = 10$ mT and -10 mT, respectively.

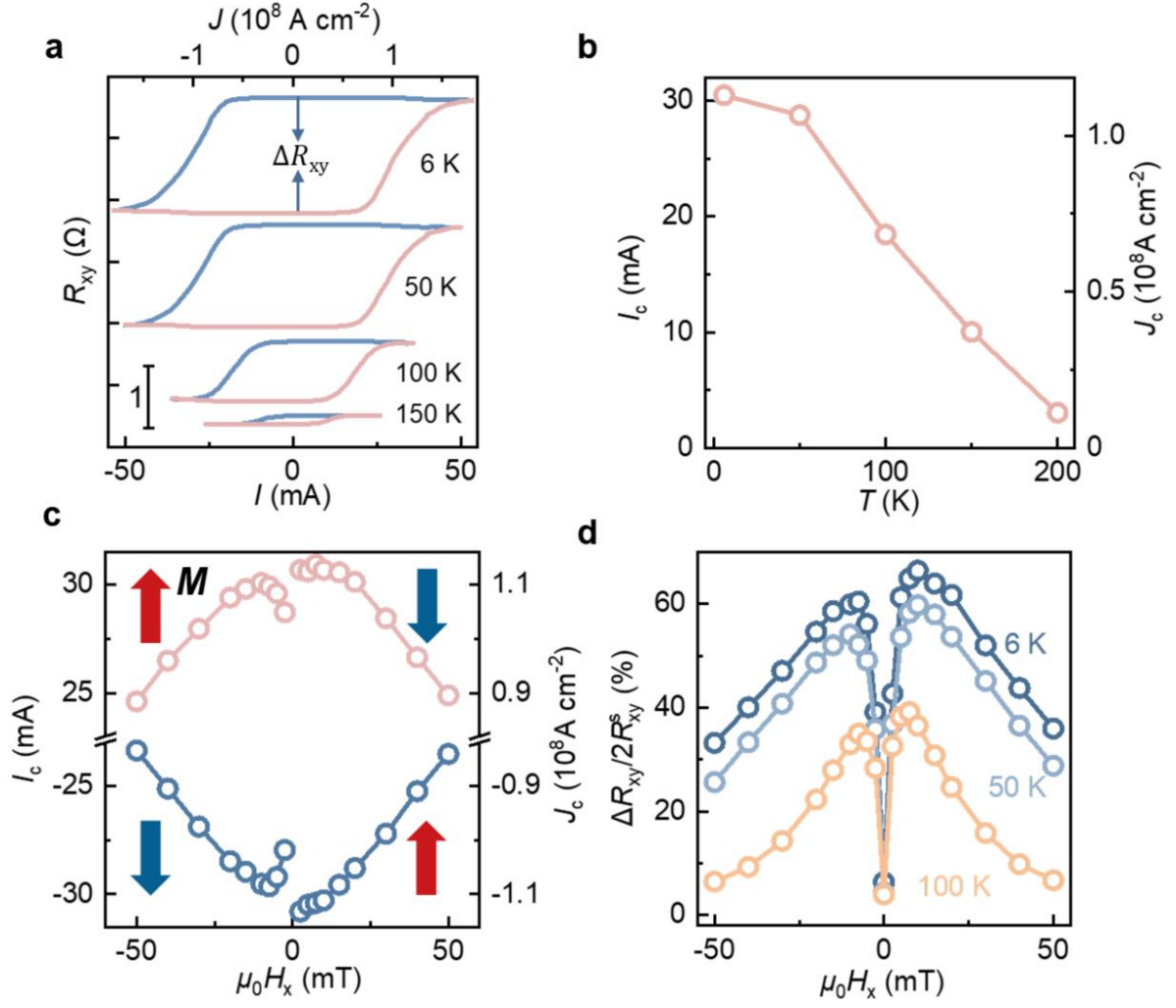


Fig. 2 | Temperature and in-plane field dependences of CIMS in Ni layer. **a**, Current-induced switching loops for Si/Ni(5.4)/NiO_x(1) at several temperatures under $\mu_0 H_x = 10$ mT. **b**, Temperature dependence of critical current I_c and critical current density J_c at 10 mT. **c**, H_x dependence of critical current I_c . **d**, H_x dependence of current-induced switching ratio $\Delta R_{xy}/2R_{xy}^s$ at several temperatures.

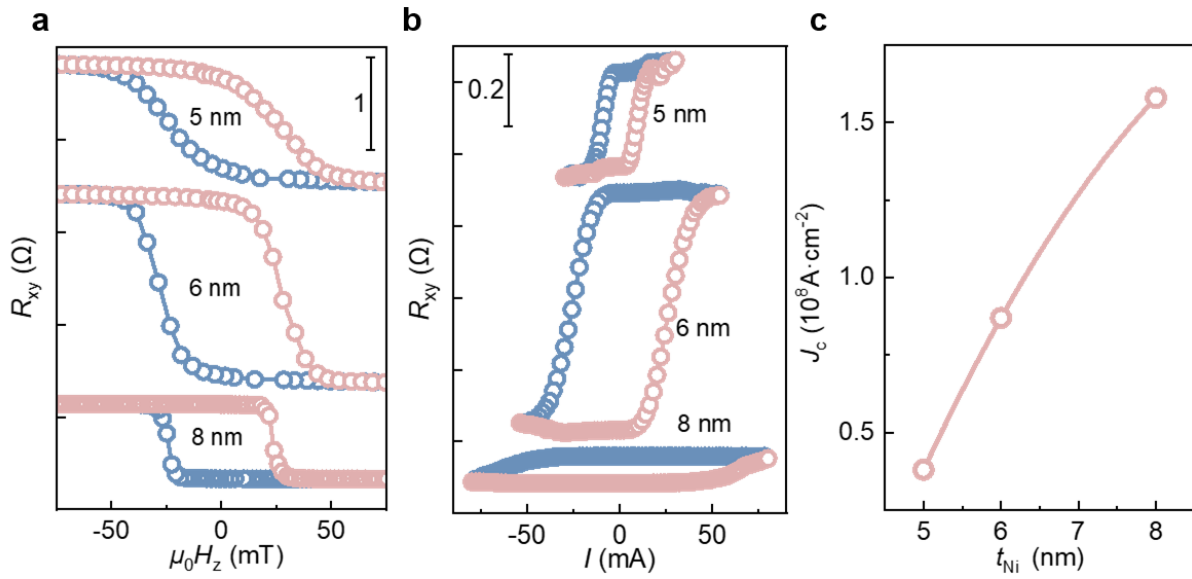


Fig. 3 | Ni thickness dependence of CIMS. a, Anomalous Hall resistance loops under out-of-plane magnetic field at 6 K for the $\text{Ni}(t_{\text{Ni}})/\text{AlO}_x(3)$ devices with several Ni thickness t_{Ni} . **b,** Current-induced switching loops of $\text{Ni}(t_{\text{Ni}})/\text{AlO}_x(3)$ with $\mu_0 H_x = 10$ mT at 6 K. **c,** Ni thickness dependence of critical current density with $\mu_0 H_x = 10$ mT at 6 K.

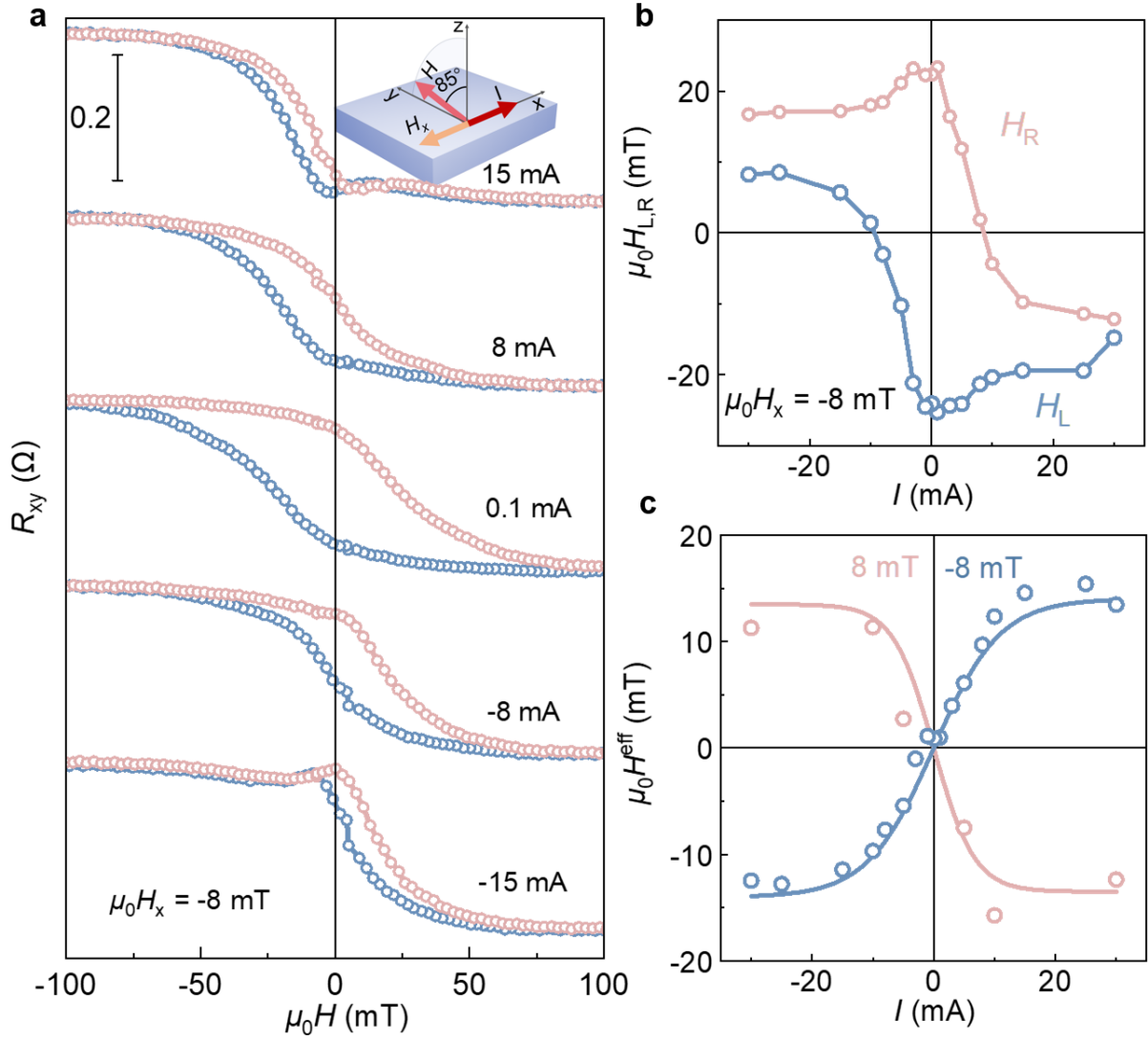


Fig. 4 | Current-induced effective magnetic fields in Ni. **a**, Anomalous Hall loops of Ni(5.4)/NiO_x(1) with varying fields at $\theta = 85^\circ$ to the normal of surface in yz plane for several currents under $\mu_0 H_x = -8$ mT at 14 K. **b**, Current dependence of switching fields H_L (field descending branch) and H_R (field ascending branch) at $\theta = 85^\circ$ with $\mu_0 H_x = -8$ mT. **c**, Current dependence of effective field H^{eff} at $\theta = 85^\circ$ with $\mu_0 H_x = 8$ mT and -8 mT, respectively.

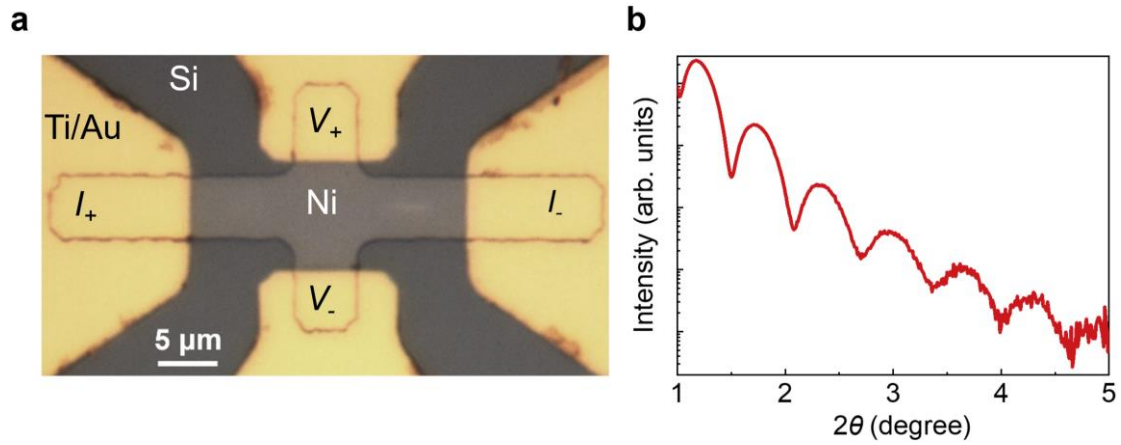


Fig. S1 | Structural characterization of the Ni device. **a**, Optical micrograph of the fabricated $20 \mu\text{m} \times 5 \mu\text{m}$ Ni Hall bar. **b**, X-ray reflectivity of a Ni film.

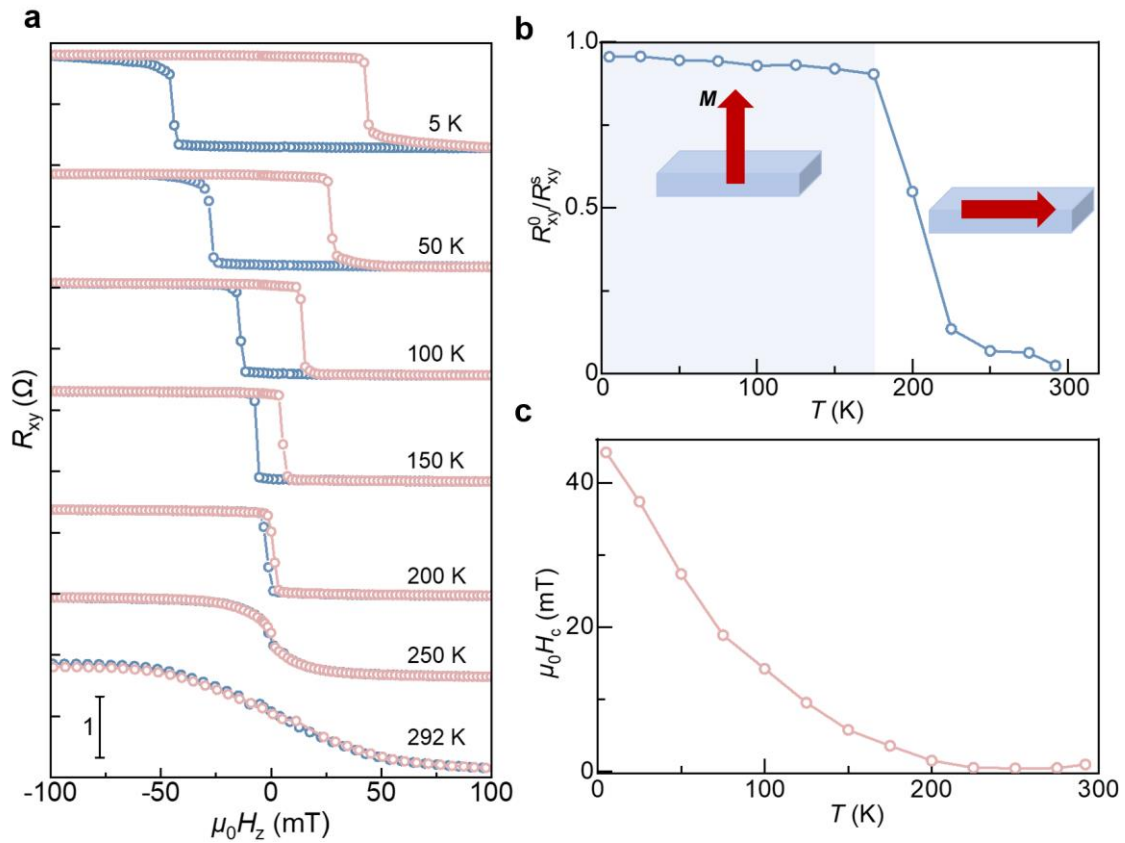


Fig. S2 | Temperature dependence of anomalous Hall resistance and coercivity in Ni/NiO_x. **a**, Anomalous Hall resistance loops of Ni(5.4)/NiO_x(1) with perpendicular fields at various temperatures. **b**, Temperature dependence of anomalous Hall remanence R_{xy}^0 / R_{xy}^s . **c**, Temperature dependence of coercive field.

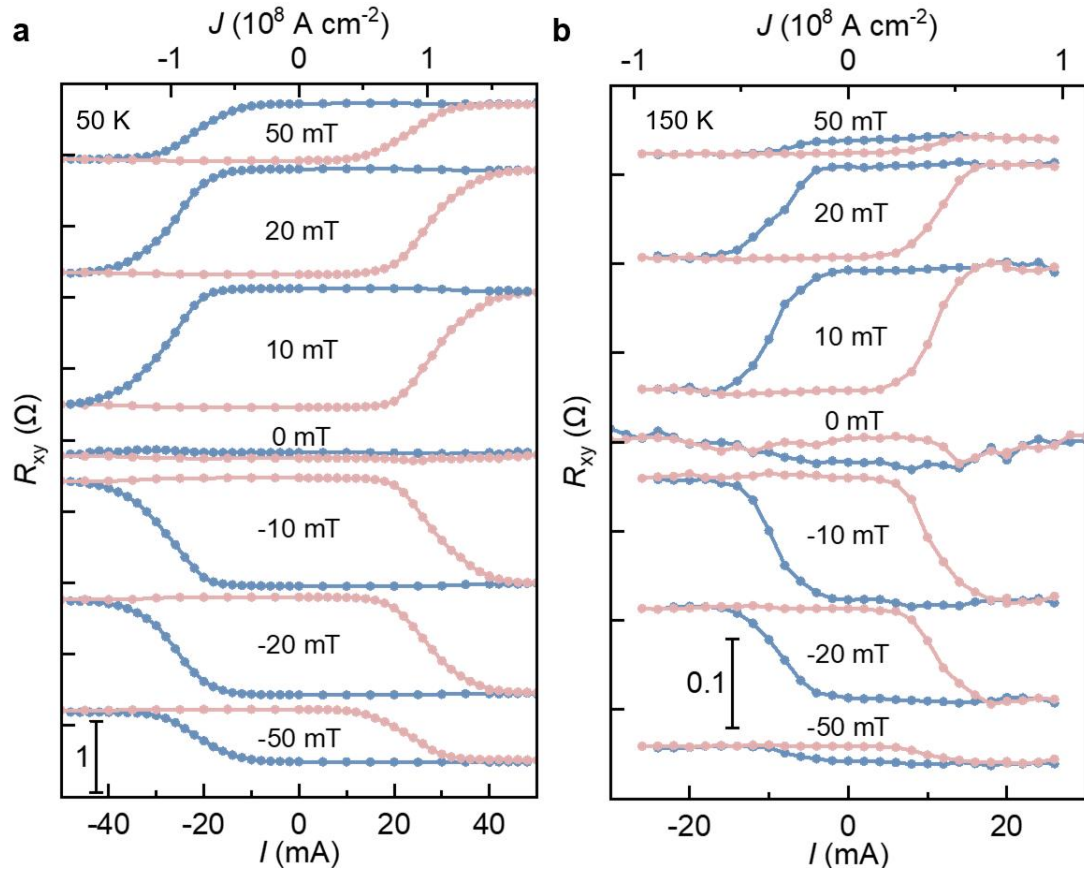


Fig. S3 | CIMS loops of Ni for several in-plane fields. Current-induced switching loops of Ni(5.4)/NiO_x(1) for several H_x at 50 K (a) and 150 K (b), respectively.

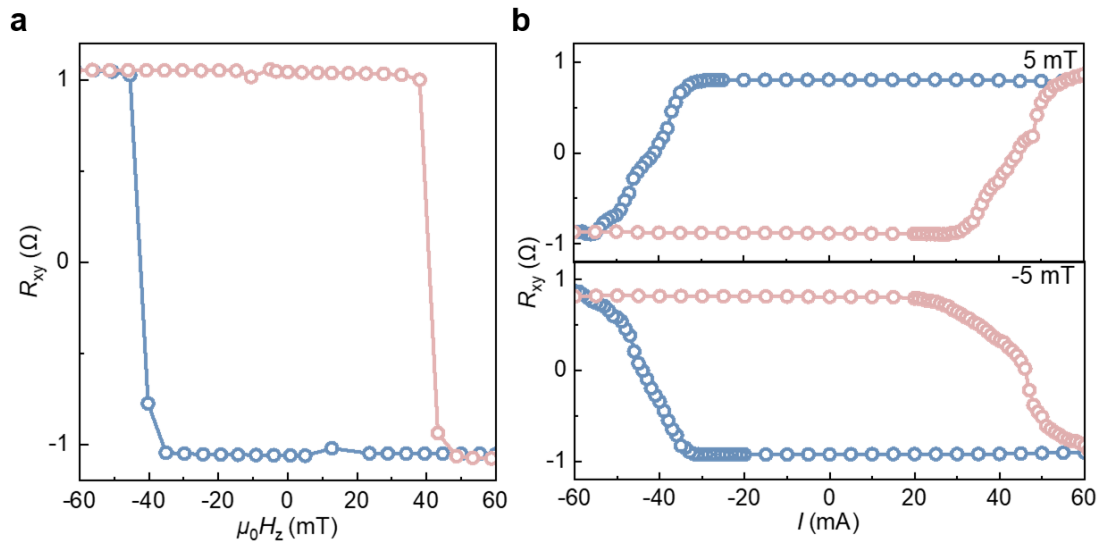


Fig. S4 | Full magnetization switching induced by current in Ni. a, Anomalous Hall resistance loop with perpendicular field at 6 K for Si/Ni(5.4)/NiO_x(1). b, CIMS loops for Si/Ni(5.4)/NiO_x(1) at 6 K with $\mu_0 H_x = \pm 5 \text{ mT}$.

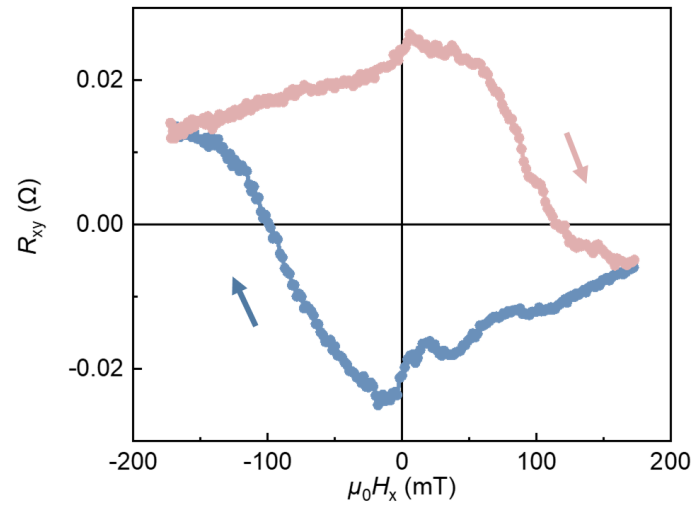


Fig. S5 | Hall loop after field cooling. Hall loop of Ni(6)/NiO_x(5) with magnetic field along x axis at 6 K and 0.1 mA after cooling under 200 mT field along +x direction. The absence of exchange bias indicates that the NiO_x is not antiferromagnetic.

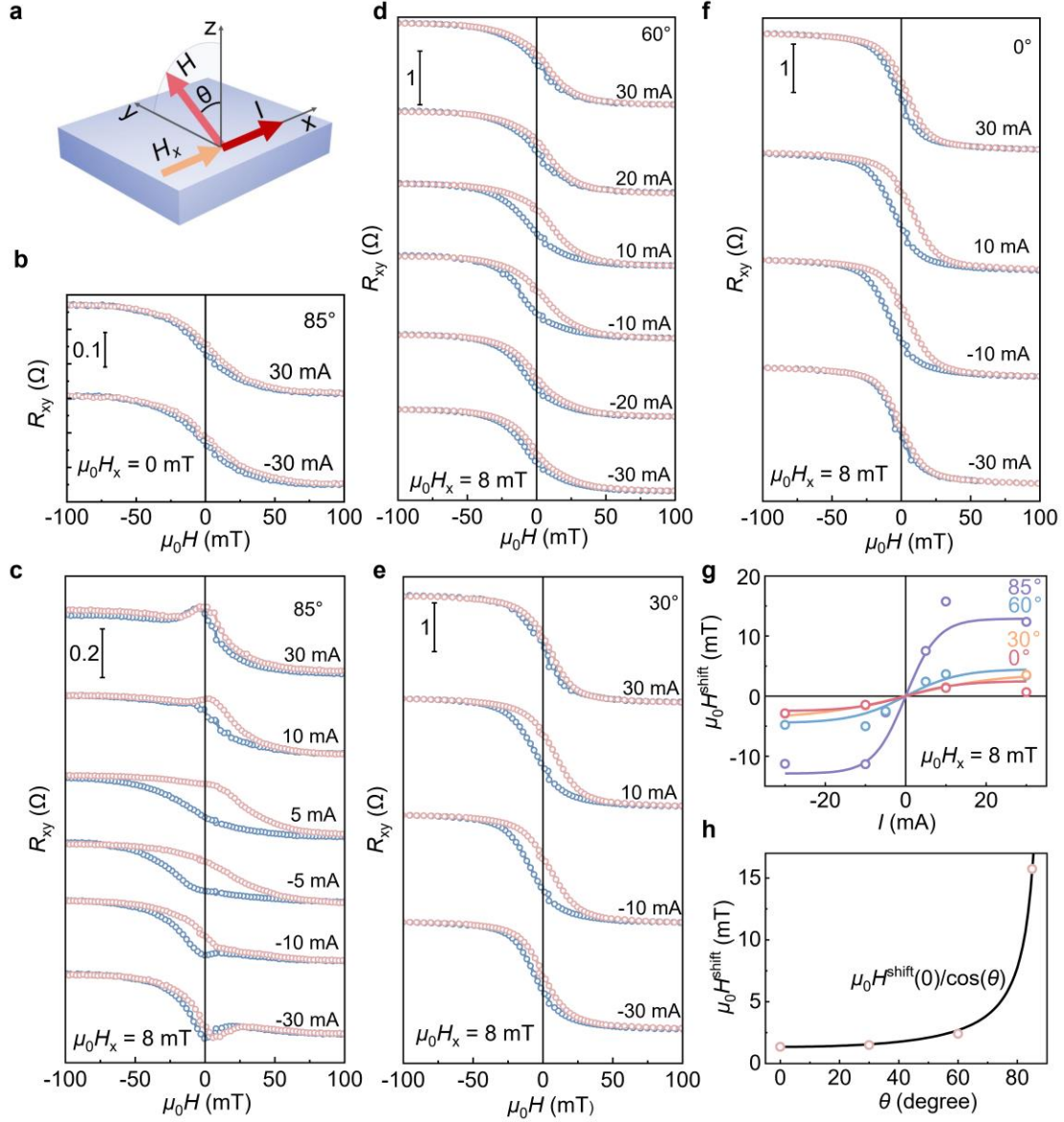


Fig. S6 | Angle dependence of current-induced anomalous Hall loop shift at 14 K. a, Schematic of the measurement of the current-induced anomalous Hall loop shift with sweeping the field at the angle θ . θ is the angle of the applied field H relative to the normal of the surface in yz plane. **b,** Anomalous Hall loops of the Ni(5.4)/NiO_x(1) with varying the field at $\theta = 85^\circ$ for several currents without the H_x . **c, d, e, f,** Anomalous Hall loops of the Ni(5.4)/NiO_x(1) with varying the field at $\theta = 85^\circ$ (**c**), 60° (**d**), 30° (**e**), and 0° (**f**) for several currents under an applied field $\mu_0 H_x = 8$ mT. **g,** Current dependence of switching fields under $\mu_0 H_x = 8$ mT at several angles θ . **h,** Angle dependence of the $\mu_0 H^{\text{shift}}$ under $\mu_0 H_x = 8$ mT and $I = 10$ mA. The solid line represents the fitting to $\mu_0 H^{\text{shift}}(0)/\cos(\theta)$.

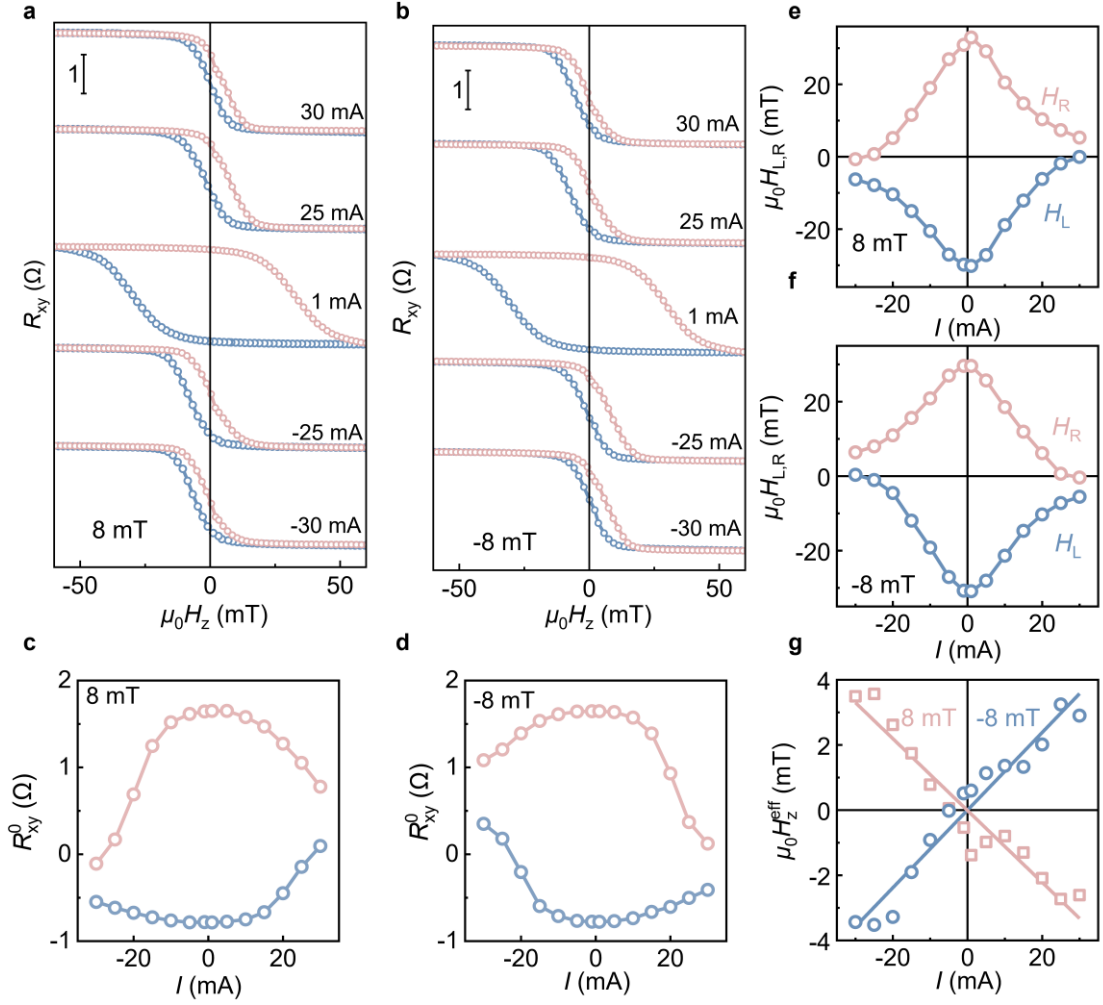


Fig. S7 | Current-induced anomalous Hall loop shift with varying perpendicular field at 6 K. **a, b**, Anomalous Hall loops of Ni(5.4)/NiO_x(1) with varying perpendicular field for several currents under an applied field $\mu_0 H_x = 8$ mT (**a**) and -8 mT (**b**), respectively. **c, d**, Current dependence of anomalous Hall resistance at zero out-of-plane field R_{xy}^0 with $\mu_0 H_x = -8$ mT (**c**) and 8 mT (**d**), respectively. **e, f**, Current dependence of switching fields H_L and H_R under $\mu_0 H_x = 8$ mT (**e**) and -8 mT (**f**), respectively. **g**, Current dependence of H_z^{eff} with $\mu_0 H_x = 8$ mT and -8 mT, respectively. The solid line represents the linear fitting to the data.

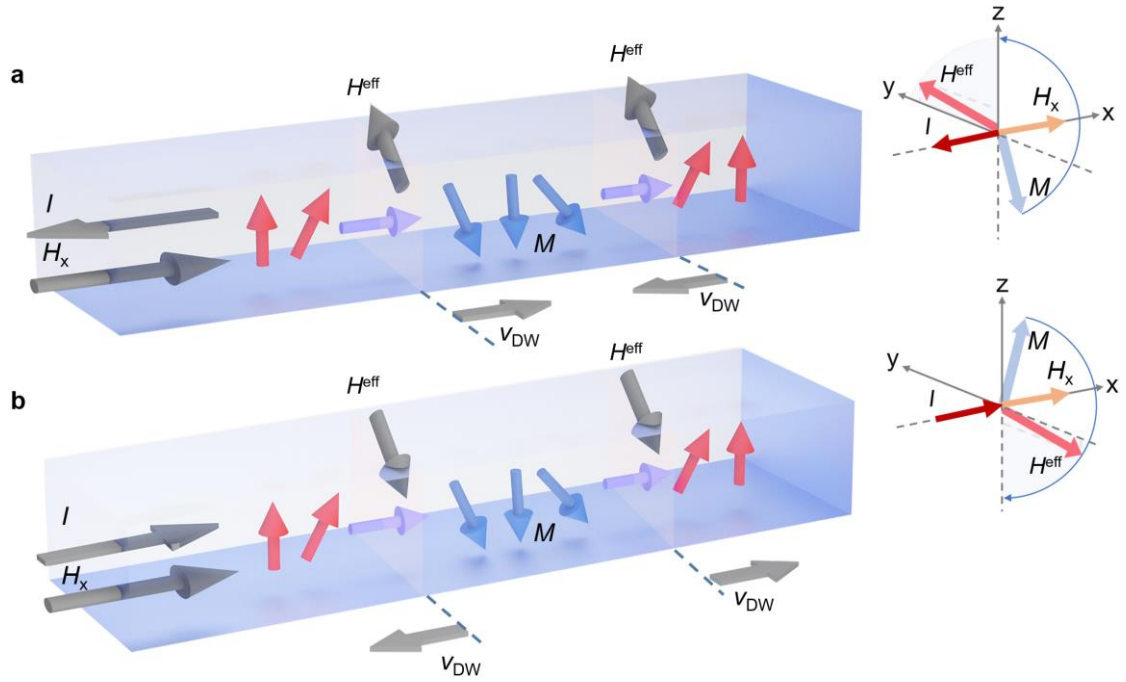


Fig. S8 | Schematic of current-induced effective field. **a**, The current-induced effective field H^{eff} around domain walls points close to the $+y$ direction with a $+z$ component as the current is along $-x$ direction with a magnetic field applied along the $+x$ direction. The magnetization-up domains expand. **b**, H^{eff} points close to the $-y$ direction with a $-z$ component as the current is along $+x$ direction with a magnetic field applied along the $+x$ direction. The magnetization-down domains expand.